Nonlinear dynamo action in a precessing cylindrical container

C. Nore[1], J. Léorat[2], J.-L. Guermond[1,3] and F. Luddens[1,3*]
[1]*Laboratoire d'Informatique pour la Mécanique et les Sciences de l'Ingénieur, CNRS UPR 3251, BP 133, 91403 Orsay cedex, France, Université Paris-Sud 11 and Institut Universitaire de France;* [2]*Luth, Observatoire de Paris-Meudon, place Janssen, 92195-Meudon, France;* [3]*Department of Mathematics, Texas A&M University 3368 TAMU, College Station, TX 77843-3368, USA*
(Dated: September 10, 2018)

It is numerically demonstrated by means of a magnetohydrodynamics (MHD) code that precession can trigger the dynamo effect in a cylindrical container. This result adds credit to the hypothesis that precession can be strong enough to be one of the sources of the dynamo action in some astrophysical bodies.

PACS numbers: 47.65.-d, 52.30.Cv, 52.65.Kj, 91.25.Cw

Simulating numerically or reproducing experimentally the dynamo action in astrophysical bodies is challenging in many respects and the question of converting kinetic energy into magnetic energy through a realistic forcing mechanism is seldom addressed either numerically or experimentally. For instance, numerical simulations are often restricted to *kinematic dynamos* where fluid flows are prescribed for simplicity reasons and bear little resemblance to reality. The three fluid dynamo experiments [1, 8, 9] that have been successful so far do not model astrophysical dynamos either, since the external pumps or internal impellers which have been used in these experiments have no astrophysical counterparts. As far as natural forcing mechanisms are concerned, buoyancy and precession are believed to be possible sources of energy for the geomagnetic dynamo. The precession hypothesis has been formulated for the first time in [7] and has since then been actively investigated from the theoretical, experimental and numerical perspectives [2, 5, 6]. To the best of our knowledge, however, it seems that it is only recently that numerical examples of precession dynamos have been reported in spheres [10, 11] and in spheroidal cavities [12]. While spheres and spheroids are relevant for planetary dynamos, cylindrical containers seem more convenient for experimental purpose. In this respect we have in mind the large scale MHD facility DRESDYN currently being built at Helmholtz-Zentrum Dresden-Rossendorf in Germany where, among other things, the action of precession will be tested on cylinders (F. Stefani, personal communication). The objective of the present Letter is to report numerical evidences supporting the idea that precession is indeed a potent mechanism to drive dynamo action in cylindrical containers.

The conducting domain considered in this letter is a cylindrical vessel $\mathcal{C}$ of radius R and length L. The vessel contains a conducting fluid and is embedded in vacuum. The solid walls of the vessel are assumed to be so thin that their influence is henceforth neglected. The container rotates about its axis of symmetry with angular velocity $\Omega_r\mathbf{e}_z$ and is assumed to precess about a second axis spanned by the unit vector $\mathbf{e}_p$ forming an angle α with $\mathbf{e}_z$, $(0<\alpha<\pi)$. The precession angular velocity is $\Omega_p\mathbf{e}_p$. A cylindrical coordinate system about the axis of the cylinder is defined as follows: the origin of the coordinate system is the center of mass of the cylinder, say O; the Oz axis is the line passing through O and parallel to $\mathbf{e}_z$; the origin of the angular coordinate $\theta\,(0\le\theta\le\pi)$ is the half plane passing through O, spanned by $\mathbf{e}_z$ and $\mathbf{e}_p$, and containing $\Omega_p\mathbf{e}_p$. The third coordinate, denoted r, is the distance to the Oz axis.

We denote by $\mathcal{L}=R$ and $\mathcal{U}=R\Omega_r$ the reference length and velocity scales, respectively. The fluid density, ρ, is assumed to be constant and the reference pressure scale is $\mathcal{P}:=\rho\mathcal{U}^2$. The magnetic permeability is uniform throughout the entire space, μ_0, and the electric conductivity of the conducting fluid is constant, σ_0. The quantities μ_0 and σ_0 are used as reference magnetic permeability and electric conductivity, respectively. The reference scale for the magnetic field is chosen so that the reference Alfvén speed is 1, i.e., $\mathcal{H}:=\mathcal{U}\sqrt{\rho/\mu_0}$. We are left with five non-dimensional parameters: one geometrical parameter L/R (aspect ratio); two forcing parameters α (precession angle) and $\varepsilon=\Omega_p/\Omega_r$ (precession rate); and two fluid parameters, namely the Ekman number $E=\nu/R^2\Omega_r$ (where ν is the kinematic viscosity) and the magnetic Prandtl number $Pm=\nu\mu_0\sigma_0$. We finally define the kinetic Reynolds number $Re=1/E$ and the magnetic Reynolds number $Rm=PmRe$.

The non-dimensional set of equations that we consider is written as follows in the precessing frame of reference:

$$\begin{aligned}\partial_t\mathbf{u}+(\mathbf{u}\cdot\nabla)\mathbf{u}+2\varepsilon\mathbf{e}_p\times\mathbf{u}+\nabla p &= \frac{1}{Re}\Delta\mathbf{u}+\mathbf{f},\\ \nabla\cdot\mathbf{u} &= 0,\\ \partial_t\mathbf{h}-\nabla\times(\mathbf{u}\times\mathbf{h}) &= \frac{1}{Rm}\Delta\mathbf{h},\\ \nabla\cdot\mathbf{h} &= 0,\end{aligned}$$

where $\mathbf{u}$, p, and $\mathbf{h}$ are the velocity field, the pressure, and the magnetic field, respectively. In the following

we consider three different modes to solve these equations: (i) The incompressible Navier-Stokes mode; (ii) The Maxwell or kinematic dynamo mode; (iii) The nonlinear magnetohydrodynamics mode (MHD). In Navier-Stokes mode the source term $\mathbf{f}$ is set to zero and $\mathbf{h}$ is not computed. In Maxwell mode, only the induction equation is solved assuming that the velocity field $\mathbf{u}$ is given. In MHD mode the full set of equations is solved and the source term $\mathbf{f}$ is the Lorentz force per unit mass, $\mathbf{f} := (\nabla\times\mathbf{h})\times\mathbf{h}$. The no-slip boundary condition on the velocity field is written as follows in the precessing frame of reference: $\mathbf{u} = \mathbf{e}_\theta$ at $r = 1$ and $\mathbf{u} = r\mathbf{e}_\theta$ at $z = \pm 1$. The magnetic field is represented as the gradient of a scalar potential in the vacuum, $\nabla\phi$. The magnetic boundary transmission conditions enforce that the magnetic field is continuous across the walls of the vessel, say Σ, i.e., $\mathbf{h}|_\Sigma = \nabla\phi|_\Sigma$.

The above equations are solved numerically by means of a code which is specialized to axisymmetric domains and has been presented in details in [3, 4]. The code is called SFEMaNS for Spectral/Finite Elements for Maxwell and Navier-Stokes equations. It is an hybrid algorithm that uses finite element representations in the meridian section of the axisymmetric domain and Fourier representations in the azimuthal direction. The magnetic field is represented as a vector field in the conducting region and as the gradient of a scalar potential in the insulating region. SFEMaNS can account for discontinuous distributions of electric conductivity or magnetic permeability and all the required continuity conditions across the interfaces are enforced using an interior penalty technique. The solution technique is parallel and parallelization is done with respect to the Fourier modes.

The typical spatial resolution in the meridional plane of the conducting domain is $\Delta x = 1/160$. We take 32 Fourier modes ($m = 0, \ldots, 31$) for Navier-Stokes runs and 64 Fourier modes ($m = 0, \ldots, 63$) for MHD runs. The typical time-step is $\Delta t = 0.001$. The grid is non-uniform in the vacuum with $\Delta x = 1/160$ at the cylinder walls and $\Delta x = 1$ at the outer boundary of the numerical domain, which is a sphere of radius ten times larger than that of the cylinder. A typical MHD run requires about 1000 CPU hours per rotation on 64 processors on an IBM-SP6.

Let us first briefly recall what is observed in a typical precessing fluid experiment starting with the fluid at rest, (see e.g. [5, 6]). The vessel is first set in rotation without precession. The fluid motion is then governed by the formation of a viscous Ekman boundary layer during the acceleration ramp. The resulting flow is a stable solid rotation independently of the strength of the acceleration phase. Once precession is applied, the Coriolis force generates an axial motion of the flow supported by the Fourier mode $m = 1$. When Re is large enough, the flow undergoes a transition from laminar to turbulent even for small precession rates and small angles [5]. The range $\varepsilon \in [0.1, 0.15]$ has been shown in [6] to maximize the ratio of axial to transverse energy in a cylinder of aspect ratio 2 in the range $Rm \in [500, 5000]$ when $\alpha = \pi/2$. Although a detailed study of the various transitions between these hydrodynamic regimes is interesting per se, due to limited numerical resource we reduce the dimensionality of the parametric space to one aspect ratio, $L/R = 2$, one precession angle, $\alpha = \pi/2$, one precession rate, $\varepsilon = 0.15$, and only two values of $Re \in \{1000, 1200\}$ and four values of $Rm \in \{600, 800, 1200, 2400\}$.

We start our investigations with a Navier-Stokes run at $Re = 1000$. The initial velocity field is the solid rotation in the precessing frame: $\mathbf{u}_0 = \mathbf{e}_z\times\mathbf{r}$. The onset of the axial circulation induced by precession is monitored by recording the time evolution of the normalized total kinetic energy $K(t) = \frac{1}{2}\int_{\mathcal{C}} \mathbf{u}^2(\mathbf{r}, t)\,\mathrm{d}\mathbf{r}/K_0$ and normalized axial kinetic energy $K_z(t) = \frac{1}{2}\int_{\mathcal{C}} u_z^2(\mathbf{r}, t)\,\mathrm{d}\mathbf{r}/K_0$ where $K_0 = \frac{1}{2}\int_{\mathcal{C}} \mathbf{u}_0^2\,\mathrm{d}\mathbf{r}$ is the kinetic energy of the initial motion. The time evolution of $K(t)$ and $K_z(t)$ for $t \in [0, 272]$ is reported in fig. 1. The time $t = 272$ corresponds to 43.3 rotation periods. After a transient that lasts 5 rotation periods and peaks at two rotation periods, the axial kinetic energy reaches a plateau value $K_z \approx 0.1$. Meanwhile, the total kinetic energy decreases and reaches a plateau value $K \approx 0.42$ after 5 rotation periods also. To enrich the dynamics of the system we have restarted the computation at $t = 72$ (i.e., 11.5 rotation periods) and increased the Reynolds number to $Re = 1200$. The time evolution of $K(t)$ and $K_z(t)$ for $t \in [72, 342]$ and $Re = 1200$ is also reported in fig. 1. The time evolution of the total kinetic energy shown in fig. 1(c) presents doubly periodic oscillations with one long period of about 8 rotation periods and one small period of about one rotation period. The short period oscillations correspond to energy exchanges between the north and south halves of the container, with a period of 2 rotation periods. The energy exchange mechanism is visible in fig. 1(d) where we have reported the time evolution of the kinetic energy of the north and south halves of the cylinder for $t \in [312, 342]$. Similar oscillations between north and south hemispheres have been reported to occur in a spheroidal cavity in [12].

We now solve the full MHD system using as initial velocity field the velocity computed at $t = 192$ during the Navier-Stokes run at $Re = 1200$. The initial magnetic field is defined as follows to trigger efficiently the dynamo instability. For the Fourier modes $m \in \{0, 1\}$, the homogeneous Dirichlet boundary condition on the scalar potential ϕ is replaced by $\phi = 0.05 z f(t)$ for $m = 0$ and $\phi = 0.05 r f(t)$ for $m = 1$, where $f(t) = \frac{\tau_a^3}{1+\tau_a^3}\left(1 - \frac{\tau_e^4}{1+\tau_e^4}\right)$ with $\tau_a = \frac{t}{0.4}$ and $\tau_e = \frac{t}{2}$. For $m \geq 2$, the amplitude of each Fourier mode of the initial magnetic field components is set to 10^{-5}. Various MHD runs are done at $Re = 1200$ for different values of the magnetic Prandtl number. The onset of dynamo action is monitored by

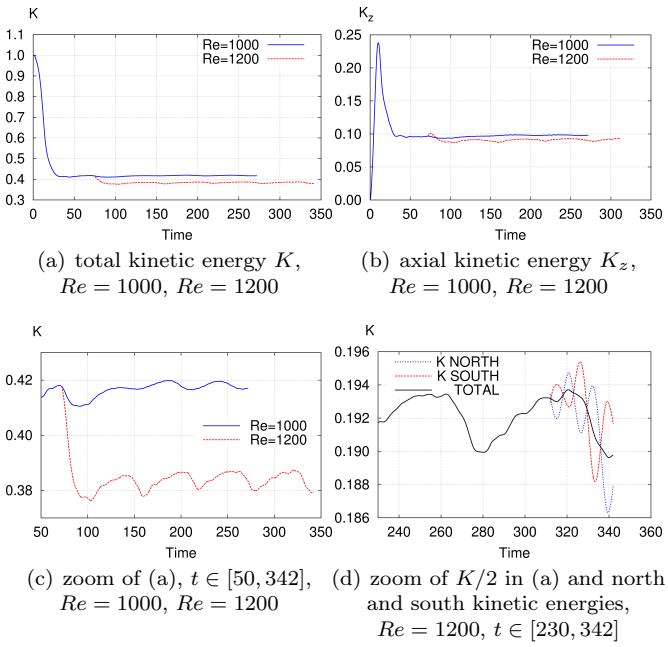

(a) total kinetic energy K, $Re = 1000$, $Re = 1200$

(b) axial kinetic energy K_z, $Re = 1000$, $Re = 1200$

(c) zoom of (a), $t \in [50, 342]$, $Re = 1000$, $Re = 1200$

(d) zoom of $K/2$ in (a) and north and south kinetic energies, $Re = 1200$, $t \in [230, 342]$

Figure 1: Time evolution of the total kinetic energy K, axial kinetic energy K_z, and total north and south kinetic energies as indicated.

recording the time evolution of the magnetic energy in the conducting fluid, $M(t) = \frac{1}{2}\int_{\mathcal{C}} \mathbf{h}^2(\mathbf{r}, t)d\mathbf{r}/K_0$. Dynamo action occurs when $M(t)$ is an increasing function of time for large times. The time evolution of M for $Pm \in \{2, 1, \frac{2}{3}, \frac{1}{2}\}$ are shown in fig. 2(a). The runs at $Pm \in \{1, \frac{2}{3}, \frac{1}{2}\}$ are done by using the velocity and magnetic fields obtained from the run $Pm = 2$ at $t = 211$ as initial velocity and magnetic fields. The flow is above dynamo threshold for $Pm = 1$ and $Pm = \frac{2}{3}$ but is subcritical for $Pm = \frac{1}{2}$. Linear interpolation of the growth-rates gives the critical magnetic Prandtl number $Pm^* \approx 0.625$ corresponding to the critical magnetic Reynolds number $Rm^* \approx 750$.

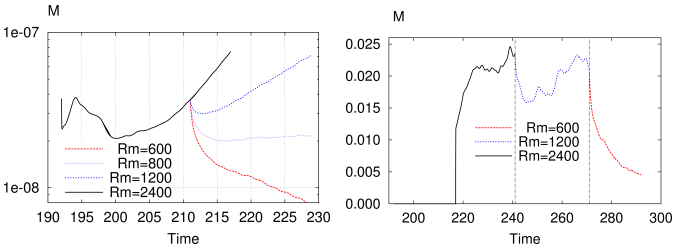

(a) linear regime

(b) nonlinear regime

Figure 2: Time evolution of the magnetic energy M in the conducting fluid (a) in the linear regime from $t = 192$ for $Re = 1200$ and various Rm as indicated (in lin-log scale) and (b) in the nonlinear regime from $t = 192$ to $t = 241$ ($Re = 1200$, $Rm = 2400$), from $t = 241$ to $t = 271$ ($Re = 1200$, $Rm = 1200$) and from $t = 271$ to $t = 292$ ($Re = 1200$, $Rm = 600$).

We now wish to observe the nonlinear saturation and evaluate the impact of the magnetic Prandtl number on the nonlinear regime. To reach nonlinear saturation in reasonable CPU time, we have used as initial data for the velocity and magnetic fields the velocity and magnetic fields from the MHD run $Pm = 2$ at $t = 217$. The velocity field has been kept unchanged but we have multiplied by 300 the amplitude of the Fourier modes $m = 0, \ldots, 5$ of the magnetic field. The time evolution of the magnetic energy of this nonlinear run in the time interval $t \in [192, 241]$ is shown in fig. 2(b). We observe that M grows smoothly until $t = 222$ and begins to oscillate thereafter. The ratio M/K is observed to be of order 10^{-2} during the nonlinear oscillating regime. After restarting the MHD run at $t = 241$ with $Pm = 1$ and running it until $t = 271$, we observe that the dynamo is still active. After restarting the MHD run at $t = 271$ with $Pm = \frac{1}{2}$ and running it until $t = 292$, we observe that the dynamo dies in a short time lapse, indicating that the dynamo bifurcation is not sub-critical for this set of control parameters. This experiment confirms the interval $\frac{1}{2} < Pm^* < \frac{2}{3}$ for the critical magnetic Prandtl number for dynamo action which has already been observed in the linear regime.

Tilgner [10] has observed that unsteadiness and breaking of the centro-symmetry of the flow facilitate dynamo action. A similar observation has been made in [12], and dynamo action is reported therein to occur when cyclic oscillations of the kinetic energy between the north and south halves of the spheroidal cavity occur. Although the loss of centro-symmetry is not a necessary condition for dynamo action, we now want to test this idea in the present cylindrical setting.

The loss of centro-symmetry of the velocity field can be monitored by inspecting its symmetric and antisymmetric components: $\mathbf{u}_s(\mathbf{r}, t) = \frac{1}{2}(\mathbf{u}(\mathbf{r}, t) - \mathbf{u}(-\mathbf{r}, t))$ and $\mathbf{u}_a(\mathbf{r}, t) = \frac{1}{2}(\mathbf{u}(\mathbf{r}, t) + \mathbf{u}(-\mathbf{r}, t))$. In the Navier-Stokes simulations reported below, we monitor the loss of centro-symmetry by inspecting the time evolution of the asymmetric kinetic energy $K_a(t) = \frac{1}{2}\int_{\mathcal{C}} \mathbf{u}_a^2(\mathbf{r}, t)d\mathbf{r}/K_0$ and we define the asymmetry ratio $r_a(t) = K_a(t)/K(t)$. The computations reported below have been done on centro-symmetric grids, but centro-symmetry is not otherwise enforced.

The time evolution of the asymmetry ratio r_a is shown in fig. 3 for the precessing cylinder at $Re = 1200$ in the time range $t \in [72, 342]$ (dotted line). The ratio r_a varies between 0.004 and 0.01 when the nonlinear regime is well established, i.e., $t \geq 220$. In order to evaluate the impact of the dynamo on the symmetry of the flow, we have started the MHD run at $t = 192$ with $Pm = 2$ (i.e., $Rm = 2400$). The time evolution of r_a is shown in solid line in fig. 3. Note that the solid and dotted lines coincide since the dynamo regime is linear in the time interval $t \in [192, 217]$ and the magnetic field is too weak to have an impact on the energy ratio r_a. We have restarted the

MHD run at $t = 217$ after multiplying the amplitude of the magnetic field by 300 as already mentioned. The ratio r_a clearly departs from its Navier-Stokes value thereafter as seen in the figure. At saturation, r_a oscillates between 0.09 and 0.011; these values are slightly greater than those reported in [10] for a precessing sphere. We have restarted the MHD run again at $t = 241$ after reducing the value of Pm to 1, thereby reducing the magnetic Reynolds number to $Rm = 1200$. The asymmetry factor is not dramatically affected by the change, as seen on the figure. We have finally restarted the MHD run at $t = 271$ after reducing the value of the magnetic Prandtl number to $\frac{1}{2}$. As expected the dynamo dies and r_a decreases to its hydrodynamical level.

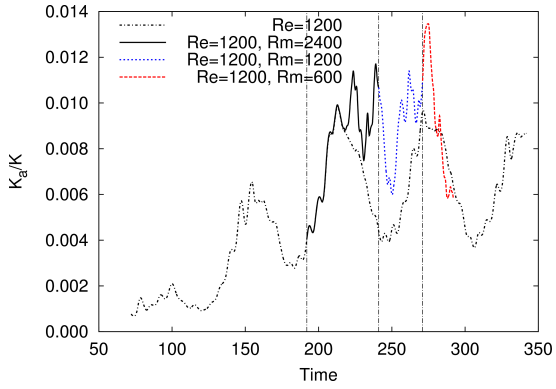

Figure 3: Time evolution of the asymmetry ratio r_a at $Re = 1200$ for $t \in [72, 342]$ in Navier-Stokes regime and $Re = 1200$, $Rm = 2400$ for $t = [192, 241]$, $Re = 1200$, $Rm = 1200$ for $t = [241, 271]$, and $Re = 1200$, $Rm = 600$ for $t = [271, 292]$ in MHD regime.

In order to study the impact of the centro-symmetry and the unsteadiness of the flow on the dynamo action, we have performed two Maxwell runs at $Rm = 1200$ with the following characteristics: (i) the velocity field at $Re = 1200$ is frozen at $t = 211$, (ii) the velocity field at $Re = 1200$ is frozen at $t = 211$ but only its symmetric component is retained so that the resulting velocity field is centro-symmetric. The time evolution of the magnetic energy of the MHD run and the two Maxwell runs (i) and (ii) are shown in fig. 4. It is remarkable that, in the two considered kinematic runs, the dynamo keeps growing with a rate similar to that of the MHD run. These computations show that neither the temporal oscillations nor the flow asymmetry play a crucial role on the dynamo action in the precessing cylinder at $Rm = 1200$.

A snapshot of the vorticity and magnetic lines at $Re = 1200$, $Rm = 2400$ is shown in fig. 5. We observe a central S-shaped vortex which is deformed by the precession and reconnects at the walls through viscous boundary layers, (see fig. 5(a)). The magnetic field lines exhibit a quadrupolar shape which is best seen in the vacuum from the top of the cylinder (see fig. 5(b)). The magnetic energy is dominated by azimuthal modes

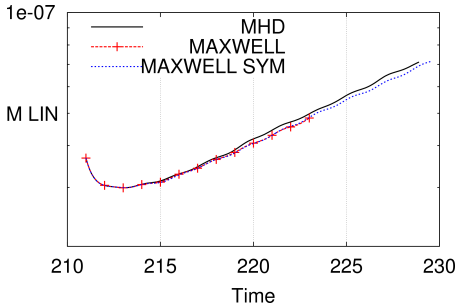

Figure 4: Time evolution of the magnetic energy M at $Re = 1200$ and $Rm = 1200$ for $t \in [211, 229]$ in MHD mode (denoted as 'MHD'), in Maxwell mode with the velocity frozen at $t = 211$ (denoted as 'MAXWELL') and in Maxwell mode with the symmetrized velocity frozen at $t = 211$ (denoted as 'MAXWELL SYM').

$m = 1, 2, 3$.

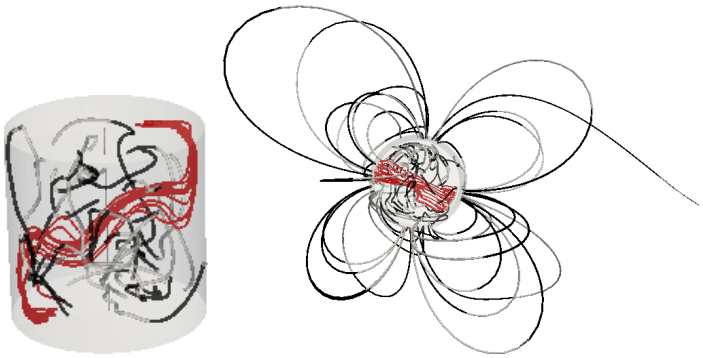

(a) from the side (b) from the top

Figure 5: Snapshot at $t = 241$ for $Re = 1200$, $Rm = 2400$ showing vorticity field lines (red) and magnetic field lines colored by the axial component in the cylinder (grey/black for positive/negative h_z component).

Forty years after the promising experiments with liquid sodium by Gans [2], we have numerically demonstrated dynamo action in a precessing cylindrical tank. The bifurcations through symmetry breaking and cyclic time dependence are similar to those already observed in dynamo flows in spherical or spheroidal precession driven cavities. There is however a large gap between the control parameters used in the present simulations and those achieved in experimental set-ups and planetary dynamos, where $E = 1/Re$ and Pm are many orders of magnitude smaller. Following this preliminary evidence for dynamo action, two further steps appear now as most urgent: (1) studying parity breaking and unsteadiness by varying the forcing parameters (precession angle and rate); (2) searching for a scaling law for the critical magnetic Reynolds number as a function of the hydrodynamic Reynolds number. Such a relation has been proposed by Tilgner in a precessing sphere [10], who argues that it

is the asymmetric part of the flow that plays a key role in the dynamo. The research program (2) will be time consuming as it will necessitate large scale computations to explore a wide range of Reynolds numbers. It will also require to develop nonlinear stabilization techniques to simulate small scale viscous dissipation. A major step in the understanding of precession dynamo will hopefully be achieved in the near future with the construction of the large scale MHD facility DRESDYN at Helmholtz-Zentrum Dresden-Rossendorf (Germany). The cooperation between simulations and experiments will lead to a better understanding of natural dynamos, including the geodynamo.

This work was performed using HPC resources from GENCI-IDRIS (Grant 2010-0254). We acknowledge fruitful discussions with D. Cébron, W. Herreman, P. Lallemand, P. H. Roberts, F. Stefani and A. Tilgner.

* Electronic address: nore@limsi.fr

[1] A. Gailitis, O. Lielausis, S. Dement'ev, E. Platacis, and A. Cifersons. Detection of a flow induced magnetic field eigenmode in the Riga dynamo facility. *Phys. Rev. Lett.*, 84:4365, 2000.

[2] R. F. Gans. On hydromagnetic precession in a cylinder. *J. Fluid Mech.*, 45:111–130, 1970.

[3] A. Giesecke, C. Nore, F. Stefani, G. Gerbeth, J. Léorat, F. Luddens, and J.-L. Guermond. Electromagnetic induction in non-uniform domains. *Geophys. Astrophys. Fluid Dyn.*, 104(5):505–529, 2010.

[4] J.-L. Guermond, R. Laguerre, J. Léorat, and C. Nore. Nonlinear magnetohydrodynamics in axisymmetric heterogeneous domains using a Fourier/finite element technique and an interior penalty method. *J. Comput. Phys.*, 228:2739–2757, 2009.

[5] R. Lagrange, C. Eloy, F. Nadal, and P. Meunier. Instability of a fluid inside a precessing cylinder. *Phys. Fluids*, 20(8):081701, 2008.

[6] J. Léorat, P. Lallemand, J.-L. Guermond, and F. Plunian. Dynamo action, between numerical experiments and liquid sodium devices. In P. Chossat, D. Armbruster, and I. Oprea, editors, *Dynamo and dynamics, a Mathematical challenge*, volume 26 of *NATO Science Series, II Mathematics, Physics and Chemistry*, pages 25–33. Kluwer, Dordrecht, 2001.

[7] W. V. R. Malkus. Precession of the Earth as the cause of geomagnetism: Experiments lend support to the proposal that precessional torques drive the Earth's dynamo. *Science*, 160(3825):259–264, 1968.

[8] R. Monchaux, M. Berhanu, M. Bourgoin, Ph. Odier, M. Moulin, J.-F. Pinton, R. Volk, S. Fauve, N. Mordant, F. Pétrélis, A. Chiffaudel, F. Daviaud, B. Dubrulle, C. Gasquet, L. Marié, and F. Ravelet. Generation of magnetic field by a turbulent flow of liquid sodium. *Phys. Rev. Lett.*, 98:044502, 2007.

[9] R. Stieglitz and U. Müller. Experimental demonstration of a homogeneous two-scale dynamo. *Phys. Fluids*, 13:561, 2001.

[10] A. Tilgner. Precession driven dynamos. *Phys. Fluids*, 17(3):034104, 2005.

[11] A. Tilgner. Kinematic dynamos with precession driven flow in a sphere. *Geophys. Astrophys. Fluid Dyn.*, 101(1):1, 2007.

[12] C.-C. Wu and P. Roberts. On a dynamo driven by topographic precession. *Geophys. Astrophys. Fluid Dyn.*, 103(6):467–501, 2009.